https://doi.org/10.5194/egusphere-2025-4648
Preprint. Discussion started: 6 October 2025

Biochar-Induced Soil Property Changes May Reduce Temperature and Precipitation Extremes: Insights from Earth System Model Experiments

Lin Yu[1], Thomas Kleinen[2], Min Jung Kwon[1], Christian Knoblauch[1], Christian Beer[1]

[1]Department of Earth System Sciences, University of Hamburg, Hamburg, 20146, Germany
[2]Department of Climate Dynamics, Max Planck Institute for Meteorology, Hamburg, 20146, Germany

Correspondence to: Lin Yu (lin.yu@uni-hamburg.de)

Abstract. Biochar has been proposed as a promising soil amendment for climate change mitigation, owing to its capacity to sequester carbon and alter soil physical properties. This study investigates the potential influence of biochar-induced changes in soil hydrological and thermal properties on future climate, with a focus on extreme climate events. We implemented a series of biochar addition scenarios (ranging from 5 to 150 t/ha) into the Max Planck Institute Earth System Model (MPI-ESM), modifying eight soil physical variables via pedo-transfer functions to investigate their impacts on climate in the near future (2040–2049) under the CMIP6 framework.

Our results show that while biochar-induced soil property changes produced minimal global effects on temperature and precipitation, they led to more structured and consistent responses in climate extremes over land. In particular, the addition of biochar reduced temperature extremes—especially nighttime minimum temperatures (TNn)—across cold regions such as Eastern Europe, the Russian Arctic, and West Siberia. Contrary to our initial hypothesis, these effects were not driven by enhanced latent heat flux but rather by increased humidity and cloud cover that altered surface energy balance via sensible heat redistribution. Precipitation extremes also responded to biochar addition, with a consistent decrease in extreme rainfall (Rx1day) over land. However, changes in consecutive dry days (CDD) were more region-specific, with increases observed in arid and coastal regions such as the Arabian Peninsula and Central Australia, indicating heightened drought risks in already vulnerable zones.

These findings suggest that although biochar's direct modifications are localized, its indirect effects on climate extremes can extend across sensitive regions through land-atmosphere interactions. Our study highlights the importance of integrating both biogeophysical and biogeochemical pathways in Earth system models to better evaluate biochar's climate mitigation potential.

1 Introduction

Climate change is intensifying the frequency and severity of extreme weather events, posing major risks to agricultural productivity and ecosystem stability (IPCC 2021). Agriculture is especially vulnerable, as shifts in temperature and precipitation directly affect yields, pest dynamics, and water availability (FAO 2023; Furtak and Wolińska 2023; Praveen and

https://doi.org/10.5194/egusphere-2025-4648
Preprint. Discussion started: 6 October 2025

Sharma 2019). This has created an urgent need for soil management strategies that strengthen resilience while contributing to climate mitigation. Increasing soil organic carbon (SOC) is particularly promising: higher SOC improves soil structure, porosity, and water retention, while also buffering temperature fluctuations—factors that enhance agricultural resilience under climate stress (Chenu, et al. 2019; IPCC 2023).

Among soil management practices, biochar has gained attention as a soil amendment that simultaneously enhances SOC and alters soil physical and chemical properties. Produced through pyrolysis, biochar adds stable SOC, improving aggregation, porosity, and water retention (Blanco-Canqui 2017; Edeh, et al. 2020; Omondi, et al. 2016; Razzaghi, et al. 2020), while also reducing thermal conductivity and diffusivity, thereby moderating soil temperature fluctuations (Usowicz, et al. 2016; Zhang, et al. 2013; Zhao, et al. 2016). In addition to these direct effects, biochar can also influence soil processes indirectly via microbial activity, root growth, and nutrient dynamics (Hossain, et al. 2020; Schmidt, et al. 2021), affecting greenhouse gas emissions (Shrestha, et al. 2023). Together, these mechanisms position biochar as a multi-dimensional modifier of the soil environment, with potential consequences for land–atmosphere interactions.

To quantify these effects, pedo-transfer functions (PTFs) are employed, using SOC levels to estimate changes in soil characteristics such as hydrological and thermal properties. These SOC-driven changes have the potential to affect climate outcomes, as soil properties directly influence the energy and water balance of the terrestrial ecosystem (Van Looy, et al. 2017). By improving water retention and moderating soil temperatures, biochar-amended soils can alter surface moisture, temperature, and evapotranspiration rates, which may subsequently impact local and regional climate dynamics, including temperature and precipitation patterns (Koster, et al. 2004; Lorenz and Lal 2014; Seneviratne, et al. 2010; Woolf, et al. 2010). Importantly, such effects may be more apparent in climate extremes—such as heatwaves, heavy rainfall, or droughts—than in mean climate conditions. Extremes often determine societal and ecological vulnerability and are more sensitive to soil moisture and surface energy fluxes (Furtak and Wolińska 2023; Grant, et al. 2025; Kwon, et al. 2025; Tian, et al. 2024).

Yet, despite extensive field studies, the biophysical climate impacts of biochar have rarely been investigated within global climate models (GCMs). First, most GCMs lack detailed representations of SOC dynamics and their influence on soil physical properties (Varney, et al. 2022). Second, the PTFs embedded in GCMs are often developed for pure mineral soils and inadequately capture SOC-related variations, leading to inaccuracies when estimating porosity, hydraulic conductivity, and thermal conductivity in SOC-rich or biochar-amended soils (Van Looy, et al. 2017). These gaps constrain our understanding of how soil management strategies may influence future climate variability and limit progress toward climate mitigation and adaptation efforts involving SOC management and biochar applications (Lehmann, et al. 2021).

Here we use the Max Planck Institute Earth System Model (MPI-ESM) to assess how biochar-induced SOC increases alter soil hydrological and thermal properties and, in turn, affect future climate—particularly climate extremes—in the near future (2040–2049). Our study focuses exclusively on biophysical pathways (changes to soil physical properties) without considering biochar's carbon sequestration effects. The experimental design comprises three steps: (1) constructing global SOC maps for multiple biochar addition scenarios by combining SOC datasets, land-use data, and application rates; (2) applying PTFs to

https://doi.org/10.5194/egusphere-2025-4648
Preprint. Discussion started: 6 October 2025

derive biochar-modified soil property maps; and (3) conducting MPI-ESM simulations to analyze changes in energy and water fluxes, near-surface climate, and extreme indices.

We hypothesize: (1) biochar addition will enhance soil porosity, leading to greater water retention and evapotranspiration, which in turn will increase latent heat flux, producing a localized cooling effect. At broader spatial scales, these localized changes may generate a weaker but detectable global cooling signal. (2) Higher biochar application rates will amplify these effects, as stronger modifications to soil hydrology and surface energy balance are expected with increasing biochar additions. (3) Consequently, we expect biochar-induced soil changes to influence future climate extremes, particularly by mitigating both temperature and precipitation extremes, with stronger impacts over land than over oceans. By explicitly testing these hypotheses in a global Earth system modeling framework, this study addresses a key gap in linking soil management, SOC dynamics, and climate extremes at scales relevant to both science and policy.

2 Model, Data, and Method

2.1 Earth System Model (MPIESM) and Experimental Setup

This study uses the Max Planck Institute Earth System Model version 1.2 in its low-resolution configuration (MPIESM1.2-LR), a state-of-the-art, fully coupled ESM employed in CMIP6 experiments (Eyring, et al. 2016; Mauritsen, et al. 2019). MPI-ESM1.2 LR couples the atmospheric component ECHAM6.3 and the land component JSBACH3.2 (200 km horizontal resolution with 47 atmospheric vertical levels) via the OASIS3-MCT coupler to the ocean model MPIOM1.6 and the ocean biogeochemistry model HAMOCC6 (150 km grid spacing and 40 vertical levels). Modifications for this study are confined to the land component, JSBACH3.2 (Reick, et al. 2021), to incorporate biochar-driven changes in soil forcing. Further details on the model structure and performance are available in Mauritsen et al. (2019).

In MPI-ESM, soil hydrological and thermal properties are provided through the land component's surface forcing file. For each experiment in this study, the default surface forcing file from the CMIP6 DECK simulations was replaced with modified soil property maps representing specific biochar addition scenarios. The modifications include adjustments to several hydrological variables—saturated hydraulic conductivity, field capacity, field saturation, wilting point, initial and maximum soil moisture, and water content in each soil layer—as well as two thermal properties: heat capacity and thermal conductivity. All properties were recalculated from SOC changes using PTFs and remained constant throughout each simulation.

A baseline (**Base**) scenario was constructed using the soil property maps generated from global soil data provided by SoilGrids (Poggio, et al. 2021), including soil texture, SOC content, water content, and bulk density. These data were applied to PTFs to calculate soil property maps, replacing the default MPI-ESM soil parameters in the surface forcing file. For the biochar addition scenarios, SOC levels were increased according to application rates ranging from 5 to 150 t ha^{-1}, and corresponding soil property maps were generated using the same PTFs. These modified maps were then incorporated into MPI-ESM to assess the climatic effects of SOC enhancement due to biochar.

https://doi.org/10.5194/egusphere-2025-4648
Preprint. Discussion started: 6 October 2025

Each biochar scenario consisted of three experiments following the CMIP6 protocol [20] and covering three simulation periods: a pre-industrial control run (***piControl***), a historical run (***historical***), and a future projection run (***future***), as illustrated in Fig. 1. The ***piControl*** run was conducted with the JSBACH standalone model over 500 years using the surface forcing file of the **Base scenario** to establish stable land conditions for soil carbon and physical properties. This steady-state land conditions from the ***piControl*** run served as the initial state for the ***historical*** simulations, together with other default initial conditions files for the CMIP6 DECK historical experiments. The ***historical*** run, performed with the fully coupled MPIESM1.2-LR, covered 1850–2014 using the **Base scenario** surface forcing file. The ***future*** runs were initialized from the end of the ***historical*** run and covered 2015–2049. Each biochar addition scenario was represented by a separate ***future*** run, using the corresponding biochar-specific surface forcing file to evaluate potential impacts on temperature and precipitation extremes.

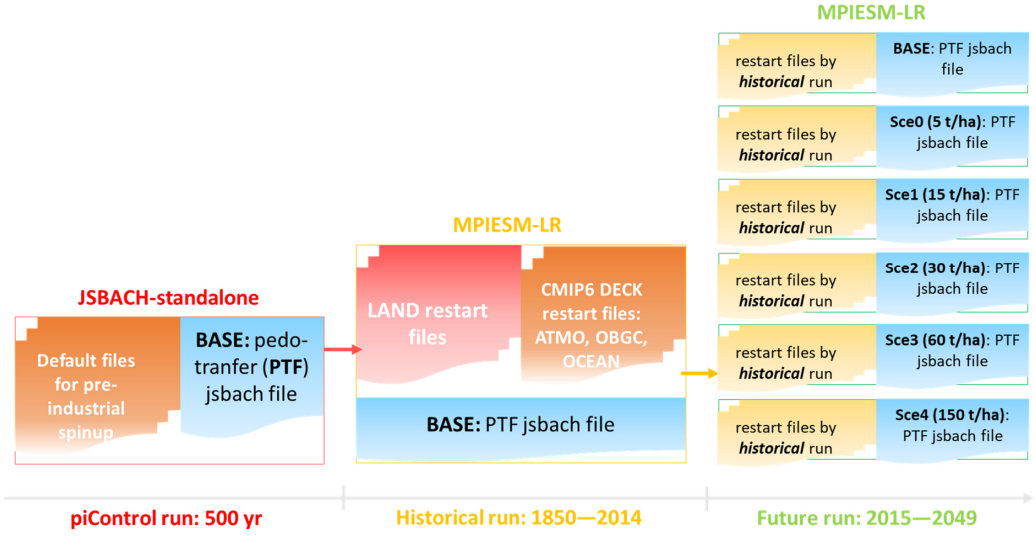

Figure 1: Schematic figure of the experiment setup. Each biochar scenario followed the CMIP6 protocol and included three simulation stages: (1) a 500-year piControl run with JSBACH-standalone to establish steady-state land conditions, (2) a coupled MPI-ESM historical run (1850–2014), and (3) future runs (2015–2049) initialized from the historical state, with biochar-specific forcing files applied in the future simulations.

2.2 Biochar addition scenarios

The biochar addition scenarios simulate a range of realistic application rates, targeting the top (0–30 cm) soil layer, where amendments are expected to have the greatest impact on soil organic carbon (SOC). Agricultural land fractions from European Space Agency Climate Change Initiative (ESA CCI) land cover data were combined with biochar application rates to represent

https://doi.org/10.5194/egusphere-2025-4648
Preprint. Discussion started: 6 October 2025

spatially explicit SOC increments in each grid cell. The procedure for incorporating these SOC changes differs between the soil property estimation step (Section 2.3) and the MPI-ESM simulations (Section 2.1).

For the generation of SOC maps used in the PTF calculations, the Base scenario (no biochar) used SOC values directly from SoilGrids without modification. For the biochar addition scenarios (Sce0: 5t/ha, Sce1: 15t/ha, Sce2: 30 t/ha, Sce3: 60 t/ha, and Sce4: 150 t/ha), the topsoil (30cm) SOC was recalculated in each grid cell according to the prescribed biochar dose and the fraction of agricultural land. These adjusted SOC values were then used in the PTFs to estimate the resulting changes in soil properties, including bulk density, thermal conductivity, and hydraulic conductivity.

In the MPI-ESM climate model simulations, only the modified soil properties generated from the PTFs were implemented. While SOC content was adjusted in the property estimation step, the MPI-ESM runs did not explicitly track SOC changes themselves. Instead, the model incorporated the derived soil property maps as the surface forcing, thereby capturing the indirect influence of biochar-induced SOC changes on climate via altered soil hydrological and thermal characteristics.

2.3 Pedo-transfer functions

Two pedo-transfer functions (PTFs) were employed to derive soil hydrological and thermal properties from basic soil data, forming the basis for the modified soil maps used in the MPI-ESM simulations.

The first PTF is based on the Community Land Model version 5 (CLM5) (Lawrence and Slater 2008), which provides a standardized framework for calculating key soil physical properties from soil texture, SOC content, and water content. This function is tailored for global-scale modeling and was used to calculate field saturation (FS), saturated hydraulic conductivity, thermal conductivity, and heat capacity. Its parameterizations ensure compatibility with global SOC datasets and enable accurate representation of soil conditions in climate simulations.

The second PTF follows the approach of Saxton and Rawls (2006), which estimates key hydrological properties—particularly those influencing soil moisture retention—based on soil texture (sand and clay percentages) and SOC content. Because the CLM5 function does not calculate field capacity (FC) or wilting point (WP), the Saxton and Rawls PTF was applied to estimate FS, FC, and WP. Ratios of FC-to-FS and WP-to-FS were then derived and used to back-calculate FC and WP based on the FS values obtained from the CLM5 function, ensuring methodological consistency.

The four soil physical properties derived directly from the CLM5 function, together with the back-calculated FC and WP values from the Saxton and Rawls approach, were incorporated into the MPI-ESM surface forcing file. This combined methodology leverages the strengths of both PTFs, ensuring a comprehensive and internally consistent estimation of soil hydrological and thermal properties for use in the climate model simulations.

2.4 Data sources and processing

Established datasets for soil characteristics and land use were used to ensure robust and regionally consistent inputs across all biochar scenarios. Soil data were obtained from SoilGrids 2.0 (Poggio, et al. 2021), a global dataset developed by ISRIC – World Soil Information, which provides predictions of soil properties at a 250 m resolution. SoilGrids 2.0 applies machine

https://doi.org/10.5194/egusphere-2025-4648
Preprint. Discussion started: 6 October 2025

learning techniques to generate global maps of soil characteristics, including soil texture and SOC content, based on harmonized soil profile data and environmental covariates. For our analysis, we accessed aggregated 5 km resolution data from the ISRIC data repository (davs://files.isric.org/soilgrids/latest/data/), ensuring comprehensive and standardized soil information for modeling. Land use data were derived from the European Space Agency's Climate Change Initiative Land Cover (CCI LC) dataset, specifically the 2020 global land cover map at 300 m resolution (Harper, et al. 2023). This dataset provides detailed land cover classifications, including agricultural regions, which are essential for estimating the spatial distribution of biochar applications and their effects on SOC.

Data processing involved selecting seven soil properties from SoilGrids required for the PTFs, including soil texture, SOC content, bulk density, and water content. These variables were aggregated into two depth layers: 0–30 cm (topsoil) and 30–200 cm (subsoil). Agricultural land fractions from the 2020 CCI LC map were aggregated from 300 m to 5 km resolution and overlaid with the topsoil SOC map. SOC increments for each biochar scenario were calculated by multiplying the agricultural land fraction in each grid cell by the prescribed biochar application rate, and these increments were added to the topsoil SOC values. Topsoil and subsoil data layers were then combined for each scenario, and the PTFs (Section 2.3) were applied to generate global soil property maps at 5 km resolution. Finally, these maps were aggregated to the T63 resolution of MPI-ESM, ensuring that soil property changes were spatially consistent with realistic land-use patterns and suitable for use in the climate simulations.

2.5 Climate Extremes Analysis

To evaluate the impacts of biochar-induced soil property changes on climate extremes, we calculated a set of widely recognized climate indices using the daily outputs from MPI-ESM simulations for the period 2040–2049. The calculations were performed with the ICCLIM (Index Calculation for CLIMate) library in Python, following the definitions and methodologies recommended by the Expert Team on Climate Change Detection and Indices (ETCCDI) (Karl, et al. 1999). We selected indices that are widely used to represent temperature and precipitation extremes and are directly relevant for assessing potential biochar impacts on extreme events.

For **temperature extremes**, two indices were considered: (1) Maximum daily maximum temperature (**TXx**), representing the hottest daytime conditions in a given period and serving as an indicator of extreme heat events and potential heatwaves. (2) Minimum daily minimum temperature (**TNn**), representing the coldest nighttime conditions in a given period and providing insights into cold extremes and frost risk. Mathematically, these are defined by Eqs. (1) and (2):

$$TXx_{kj} = max(TXx_{kj}) \quad (1)$$

$$TNn_{kj} = min(TN_{n_{kj}}) \quad (2)$$

where TXx_{kj} is the daily maximum temperature in month k, year j, and TNn_{kj} is the daily minimum temperature in month k, year j. In this study, TXx and TNn were calculated for each year from 2040 to 2049, and the decadal mean values were used in the analysis.

https://doi.org/10.5194/egusphere-2025-4648
Preprint. Discussion started: 6 October 2025

For **precipitation extremes**, two indices were calculated: (3) Maximum 1-day precipitation (**Rx1day**), representing the most intense single-day rainfall each year and associated flood risk. (4) Consecutive dry days (**CDD**), defined as maximum length of dry spell each year (i.e., the longest number of consecutive days with daily precipitation RR < 1mm), providing an indicator of drought severity and persistence. The annual Rx1day index is given by Eq. (3):

$$Rx1day_j = max(RR_{ij}) \quad (3)$$

where RR_{ij} is the daily precipitation amount on day i in period j. For CDD, the maximum number of consecutive days with RR<1 mm was identified for each year. Both Rx1day and CDD were computed annually for 2040–2049, and the results are presented as decadal means.

To assess spatial patterns and regional responses, multiple geographic masks were applied. First, agricultural and non-agricultural regions were identified by combining the agricultural land fraction from the 2020 CCI LC dataset (Section 2.4) with the MPI-ESM default land-sea mask. Second, regional masks based on the Intergovernmental Panel on Climate Change Sixth Assessment Report (IPCC AR6) Reference Land and Ocean Regions (IPCC 2021) were applied to identify key climatic zones and facilitate inter-regional comparisons (Fig. S1). This dual-masking approach allowed us to quantify the potential influence of biochar both locally (in areas where application is most likely) and globally.

By focusing on these four indices, the analysis provides a concise yet robust assessment of how biochar-induced modifications to soil hydrological and thermal properties may affect the intensity, frequency, and duration of extreme temperature and precipitation events across different spatial scales.

3 Results

3.1 Effects of Biochar Amendment on Global-scale Soil Properties

In the base scenario, the global soil organic carbon (SOC) stock in the top 30 cm of soil is estimated at 48.2 ± 23.4 t/ha (Fig. 2). Under the low-addition scenario (Sce0: 5 t/ha), SOC stocks increase modestly by 2.5 ± 2.7% across agricultural regions, with localized gains reaching up to 26.9% in SOC-poor areas. In contrast, high biochar addition (Sce4: 150 t/ha) results in a substantial increase of 60.0 ± 63.6%, with maximum increments exceeding 600% (Table 1). The medium-addition scenario (Sce2: 30 t/ha) yields an intermediate SOC increase of 15.0 ± 15.9%.

As SOC increases, soil bulk density decreases. The global mean bulk density in the base scenario is 1270 ± 179 kg/m³. Biochar addition reduces bulk density by 0.4% in the low-addition scenario, 2.1% in the medium-addition scenario, and up to 7.5% in the high-addition scenario (Fig. 2; Table 1).

The estimated global saturated hydraulic conductivity (k_sat) is 4.04 ± 2.32 × 10^{-6} m/s. With increasing biochar application, k_sat declines slightly—by 0.2%, 1.0%, and 3.6% in the low, medium, and high addition scenarios, respectively. Volume-related hydraulic properties—including field saturation, field capacity, and wilting point—all show consistent increases with biochar addition (Fig. S2; Table 1).

https://doi.org/10.5194/egusphere-2025-4648
Preprint. Discussion started: 6 October 2025

Regarding thermal properties, the global mean heat capacity is 2.69 ± 0.17 × 10^6 J/m³/K. Biochar addition leads to slight reductions of 0.05%, 0.33%, and 1.13% in the low, medium, and high scenarios, respectively. Similarly, the global mean thermal conductivity is 5.39 ± 0.87 W/m/K, decreasing by 0.17%, 1.00%, and 3.57% across the same scenarios (Fig. S2; Table 1).

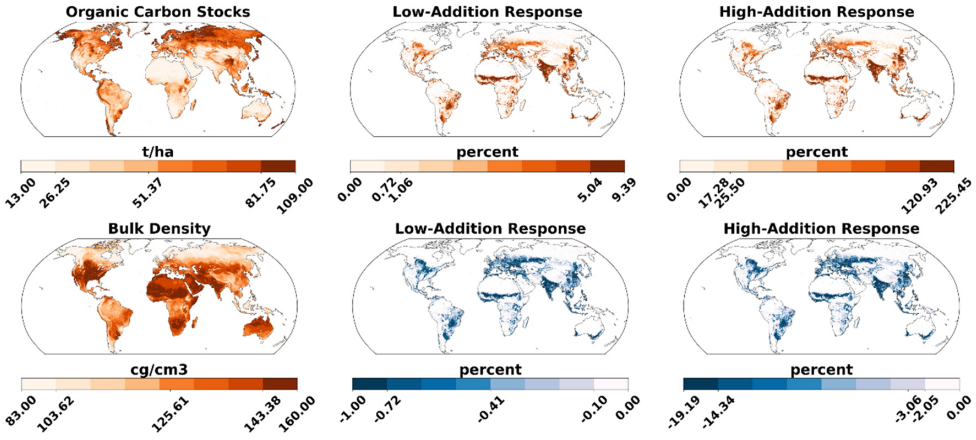

Figure 2: Global Soil Organic Carbon Stocks and Bulk Density (SoilGrids Data) and Their Percentage Changes in Response to Low (Sce0: 5 t/ha) and High (Sce4: 150 t/ha) Biochar Additions in Agricultural regions.

Table 1. Global Mean Soil Organic Carbon Stocks and Estimated Soil Properties in the Base Scenario, Along with Percentage Changes in Response to Low (5 t/ha), Medium (30 t/ha), and High (150 t/ha) Biochar Additions. The reference listed in the table are: [1] Razzaghi, et al. (2020), [2] Omondi, et al. (2016), [3] Razzaghi, et al. (2020), [4] Edeh, et al. (2020), [5] Blanco-Canqui (2017), [6] Zhao, et al. (2016), [7] Zhang, et al. (2013).

	Base scenario	5 t/ha [mean±std, p1, p999, %]	30 t/ha [%] [mean±std, p1, p999, %]	150 t/ha [%] [mean±std, p1, p999, %]	Literature [%]
Organic Carbon Stock	44.46±22.32 [t/ha]	2.59±2.72, 0.02, 14.30	15.52±16.33, 0.10, 85.82	62.08±65.32, 0.38, 343.29	NA
Bulk Density	1307±162 [kg/m3]	-0.37±0.34, -1.09, -0.00	-2.12±1.91, -6.19, -0.02	-7.54±6.50, -20.55, -0.06	-11~-7 [1] -6.5~-8.7 [2]
Permanent wilting point	0.19±0.05 [m/m]	1.67±1.65, 0.40, 6.63	2.35±2.11, 0.40, 8.50	4.46±5.07, 0.40, 24.21	-5~47 [3] -0.4~22.2 [4]

https://doi.org/10.5194/egusphere-2025-4648
Preprint. Discussion started: 6 October 2025

Field Capacity	0.34±0.08 [m/m]	0.49±0.35, 1.88	0.01,	1.28±1.49, 7.36	0.01,	3.72±5.12, 23.61	0.01,	3.5~23.9 [4] 1~51 [3]
Field Saturation	0.51±0.04 [m/m]	0.14±0.25, 0.0, 1.28		0.83±1.42, 0.0, 7.19		2.96±4.92, 23.29	0.0,	5.8~11.1 [2] 14~64 [5]
Saturated hydrological conductivity	4.21±2.45 [e-6 m/s]	-0.19±0.31, 0.0	-1.09, -0.0	-1.08±1.80, 0.0	-6.19, -0.0	-3.86±6.25, 0.0	-20.79, -0.0	13.8~37.7 [2] -64.6~36 [4]
Heat Capacity	2.65±0.16 [e6 J/ m3/K]	-0.06±0.10, 0.00	-0.37,	-0.34±0.58, 0.00	-2.11, -0.00	-1.22±2.02, 0.00	-7.20, -0.00	No effects
Thermal conductivity	5.47±0.90 [W/ m/K]	-0.19±0.31, 0.0	-1.07, -0.0	-1.07±1.78, 0.0	-6.10, -0.0	-3.81±6.17, 0.0	-20.47, -0.0	-0.3~-32.2 [6] -3.5~-7.5 [7]

3.2 Responses of the Earth System and Climate Extremes to Biochar Additions

Biochar application increased SOC and altered soil hydrological and thermal properties in a dose-dependent manner (Table 1). While these changes were systematic, their magnitudes in MPI-ESM inputs remained relatively small—typically <1% for the low-addition scenario and <5% for the high-addition scenario (Fig. 3).

Simulated global-scale changes in key water and energy balance variables were generally weak (<1%) and often non-linear (Fig. 3). In the baseline simulation (Base scenario), the global energy balance, represented by net top-of-atmosphere (TOA) radiation during 2040–2049, is 1.59 ± 55.39 W/m², indicating a pronounced planetary energy imbalance (warming). TOA radiation decreased in most biochar scenarios (−1% to −4.6%), suggesting a cooling effect, except in the medium-addition case (+1.3%). The global net freshwater flux (nfwf) in the Base scenario is 0.064 mg/m²/s (water entering the Earth's surface) and increased slightly in all but the medium scenario, which showed a 5% reduction.

Over land, responses were more coherent across scenarios (Fig. 4). Biochar consistently increased soil wetness, consistent with its effect on soil water-holding capacity, leading to general increases in evaporation (evap) and latent heat flux (ahfl). However, these increases were neither consistent nor dose-dependent. In contrast, sensible heat flux (ahfs) and cloud cover (aclcov) both decreased systematically, while near-surface relative humidity (rh2m) increased across all scenarios. Together, these changes contributed to a consistent reduction in TOA radiation over land, indicating a net cooling effect.

This coherence was even stronger in the response of climate extreme indices, with TXx, TNn, and Rx1day consistently declining over land in all scenarios (Fig. 4). Although no clear dose–response pattern emerged, higher application scenarios (≥30 t ha^{-1}) generally showed stronger reductions in TXx, TNn, and CDD than lower-dose cases (<30 t ha^{-1}).

https://doi.org/10.5194/egusphere-2025-4648
Preprint. Discussion started: 6 October 2025

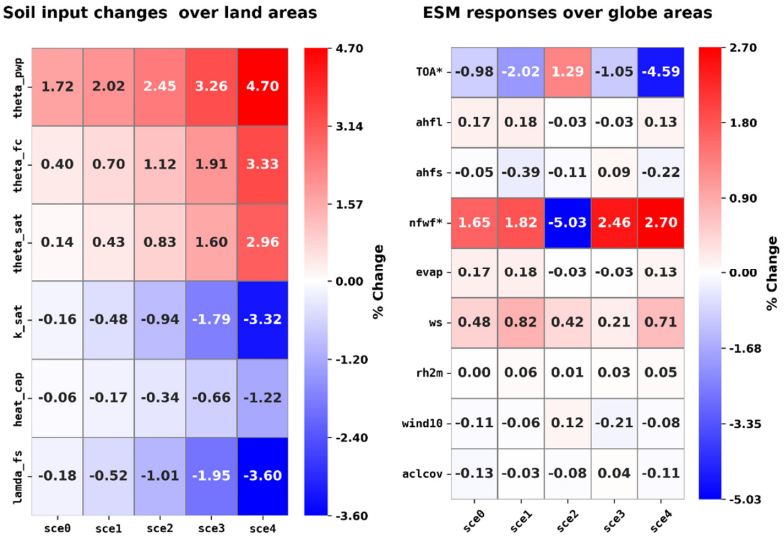

Figure 3: Percentage Changes in Soil Properties Introduced to MPI-ESM and Their Effects on Global Water and Energy Cycle Variables (2040–2049). The left panel shows percentage changes in soil physical properties introduced to the MPIESM through different biochar addition scenarios. Inputs include: theta_pwp (permanent wilting point), theta_fc (field capacity), theta_sat (field saturation), k_sat (saturated hydrological conductivity), heat_cap (heat capacity), lamda_fs (heat conductivity). The right panel presents corresponding percentage changes in key water and energy cycle variables, averaged globally over the 2040–2049 period, relative to the Base scenario. Each grid cell represents the mean change for a given variable and scenario. For variables marked with an asterisk (*), negative values indicate fluxes directed away from the land or Earth system (e.g., toward the atmosphere or space), while positive values represent incoming fluxes. Variables include: TOA (net top-of-atmosphere radiation), ahfl (latent heat flux), ahfs (sensible heat flux), nfwf* (net freshwater flux: evapotranspiration + precipitation), ws (soil wetness), rh2m (2 m relative humidity), wind10 (10 m wind speed), and aclcov (total cloud cover).

https://doi.org/10.5194/egusphere-2025-4648
Preprint. Discussion started: 6 October 2025

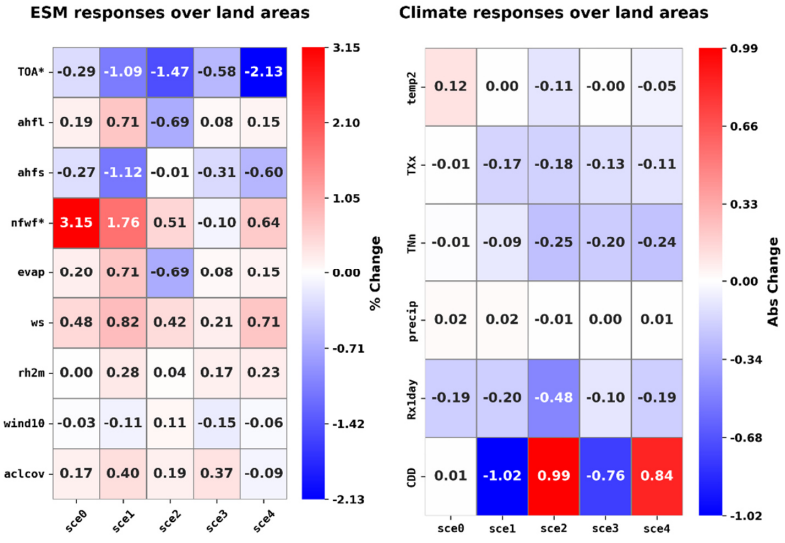

Figure 4: Responses of Water and Energy Cycle Variables in MPIESM and Temperature and Precipitation Metrics to Biochar Addition Scenarios Over Land Areas (2040–2049). The left panel presents corresponding percentage changes in key water and energy cycle variables, averaged globally over the 2040–2049 period, relative to the Base scenario. Each grid cell represents the mean change for a given variable and scenario. For variables marked with an asterisk (*), negative values indicate fluxes directed away from the land or Earth system (e.g., toward the atmosphere or space), while positive values represent incoming fluxes. Variables include: TOA (net top-of-atmosphere radiation), ahfl (latent heat flux), ahfs (sensible heat flux), nfwf* (net freshwater flux: evapotranspiration + precipitation), ws (soil wetness), rh2m (2 m relative humidity), wind10 (10 m wind speed), and aclcov (total cloud cover). The right panel displays the absolute changes in six climate variables—2 m temperature (temp2), maximum daily maximum temperature (TXx), minimum daily minimum temperature (TNn), precipitation (precip), maximum 1-day precipitation (Rx1day), and consecutive dry days (CDD)—in response to five levels of biochar addition. The left panel shows changes averaged over the entire globe, while the right panel focuses on land-only areas. Values represent mean differences between each biochar scenario and the base scenario over the 2040–2049 period.

3.3 Climate Responses under the Medium Biochar Addition Scenario

3.3.1 Temperature and Precipitation

In the Base scenario, rising atmospheric CO_2 levels lead to a gradual increase in near-surface (2m) air temperature (temp2) and precipitation over the simulation period, with marked spatial variability across regions and surface types (Figs. 5, 6). The temperature distribution in the Base scenario indicates that agricultural regions are generally warmer due to their location in temperate and tropical zones, while non-agricultural lands include colder high-latitude regions (Table 2; Fig. 6a).

In response to the medium biochar addition scenario (**Sce2**: 30 t/ha), a slight cooling effect is observed at the global scale, with a mean reduction of 0.037°C in near-surface air temperature during the period 2040–2049. This cooling is more pronounced

https://doi.org/10.5194/egusphere-2025-4648
Preprint. Discussion started: 6 October 2025

over land (−0.11°C), particularly in non-agricultural regions (−0.12°C) compared to agricultural areas (−0.087°C) (Table 2; Figs. 5b, 5d).

Precipitation responses under medium biochar addition are weaker and spatially less coherent. A small global reduction in mean daily precipitation is simulated (−0.0011 mm/day, equivalent to −0.41 mm/year), which is primarily attributed to land areas (−0.007 mm/day), with a slightly stronger reduction in non-agricultural regions compared to agricultural zones (Figs. 6b, 6d). Seasonal patterns in land precipitation remain largely unchanged, except for a slight weakening of the summer peak in agricultural regions.

3.3.2 Climate Extreme Index

Climate extremes in the Base scenario exhibit strong contrasts between land and ocean, as well as between agricultural and non-agricultural regions (Table 2). Land areas show greater diurnal temperature variability (TXx - TNn), less extreme precipitation events (Rx1day) and longer dry spells (CDD). Agricultural regions have much higher TXx and Rx1day compared to the non-agricultural regions, but also a slightly longer dry spell.

Between 2040 and 2049, TXx and TNn decrease by 0.18°C and 0.25°C over land, respectively. These reductions exceed both the global average changes (−0.05°C and −0.07°C) and the mean land surface cooling (−0.11°C) (Table 2). The reduction in TNn is relatively uniform between agricultural and non-agricultural regions, while the decline in TXx is stronger in agricultural zones.

Precipitation-related extremes show weaker and more spatially variable responses. Under medium biochar addition, Rx1day decreases by 0.48 mm over land, with a stronger signal in agricultural regions (−0.61 mm) than non-agricultural areas (−0.40 mm). CDD, in contrast, increase over land by 0.99 days, with a more pronounced increase in non-agricultural regions (+1.39 days) than the agricultural regions (+0.44 days).

https://doi.org/10.5194/egusphere-2025-4648
Preprint. Discussion started: 6 October 2025

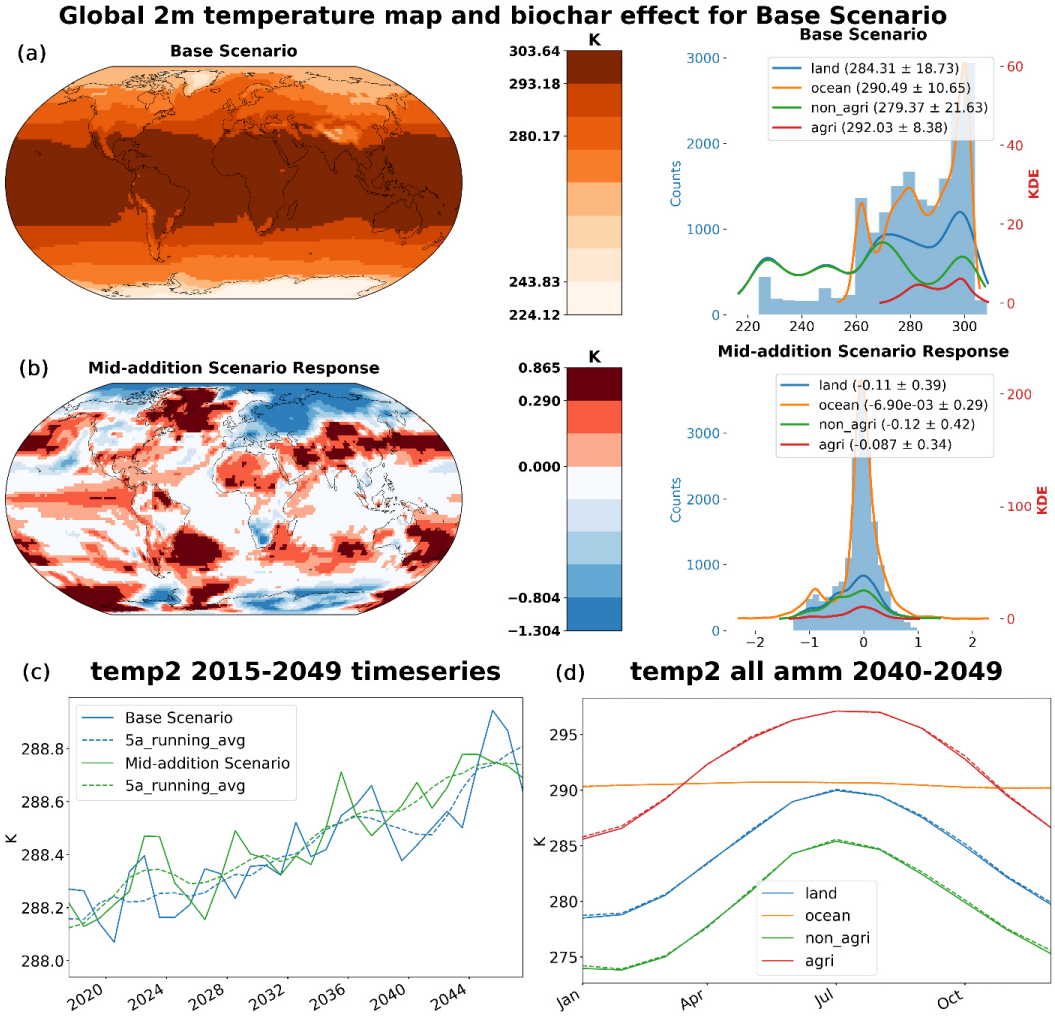

Figure 5: Simulated Global 2m Temperature and Seasonal Dynamics in the Base and Medium-Addition Biochar Scenarios. (a) Global map of simulated 2m temperature in the base scenario and distribution of temperature values across different surface types. (b) changes in global 2m temperature in response to medium biochar addition, alongside surface type distribution. (c) Global mean 2m temperature in the base scenario and medium-addition scenario (2015–2049). (d) Annual monthly mean (amm) dynamics of global mean 2m temperature in the Base (solid line) and Medium-Addition (dotted line) scenarios, separated by surface type (ocean, land, agricultural region, and non-agricultural land).

https://doi.org/10.5194/egusphere-2025-4648
Preprint. Discussion started: 6 October 2025

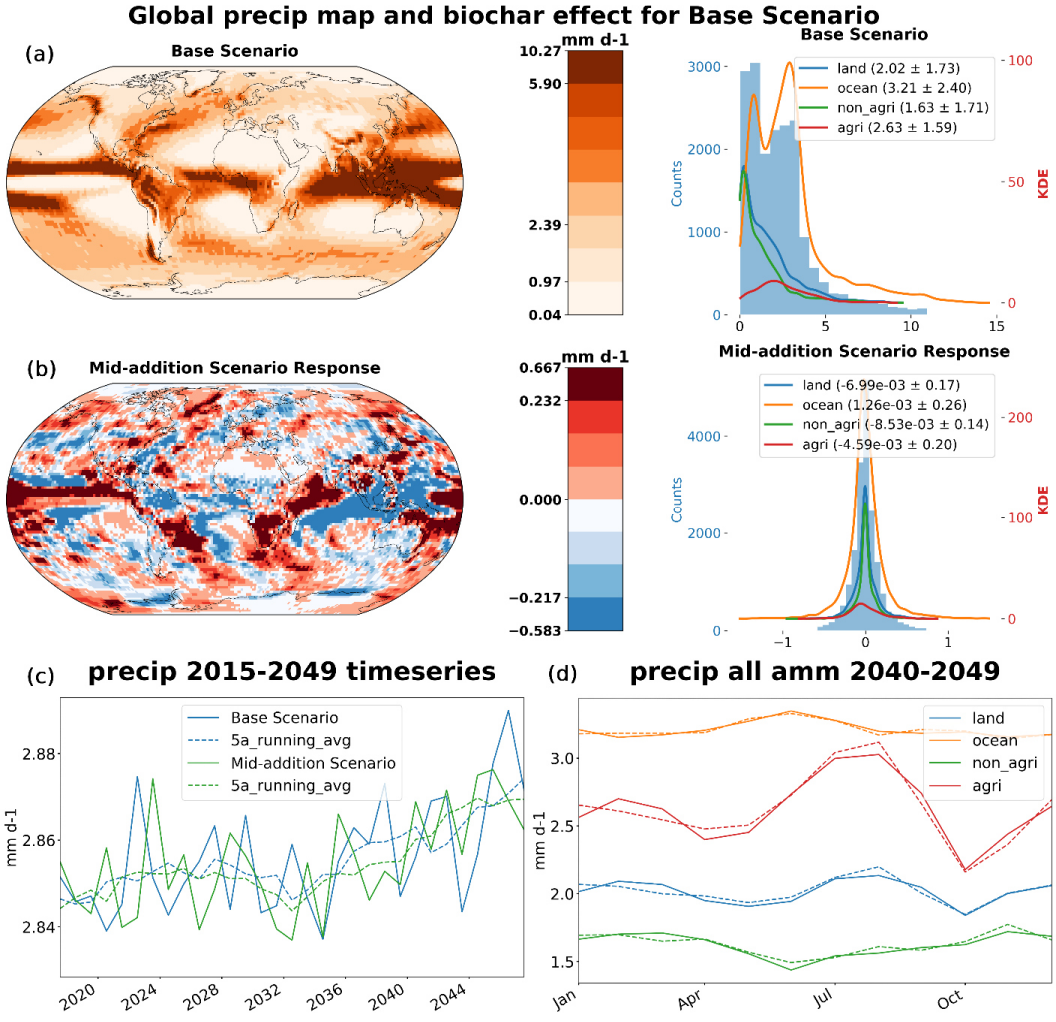

Figure 6: Simulated Global Precipitation and Seasonal Dynamics in the Base and Medium-Addition Biochar Scenarios (2040–2049). (a) Global map of simulated precipitation in the base scenario and distribution of rainfall values across different surface types. (b) changes in global precipitation in response to medium biochar addition, alongside surface type distribution. (c) Global mean precipitation in the base scenario and medium-addition scenario (2040–2049). (d) Annual monthly mean (amm) dynamics of global mean precipitation in the Base (solid line) and Mid-Addition (dotted line) scenarios, separated by surface type (ocean, land, agricultural region, and non-agricultural land).

https://doi.org/10.5194/egusphere-2025-4648
Preprint. Discussion started: 6 October 2025

Table 2. Mean Values and Biochar-Induced Responses of Temperature, Precipitation, and Climate Extremes Across Surface Types and Continents (2040–2049).

Continent \ Surface type	Temp [K] [mean, response]	TXx [°C] [mean, response]	TNn [°C] [mean, response]	Precip [mm/d] [mean, response]	Rx1day [mm] [mean, response]	CDD [days] [mean, response]
globe	288.71, **-0.04**	24.52, **-0.05**	5.09, **-0.07**	2.87, **-0.0011**	32.39, **-0.12**	52.92, **+0.51**
ocean	290.49, **-0.01**	22.52, **0.00**	10.26, **-0.00**	3.21, **0.0013**	35.24, **0.02**	43.46, **+0.33**
land	284.31, **-0.11**	29.43, **-0.18**	-7.68, **-0.25**	2.02, **-0.0070**	25.35, **-0.48**	78.46, **+0.99**
Agriculture	292.03, **-0.09**	35.10, **-0.26**	2.57, **-0.22**	1.18, **-0.0046**	31.76, **-0.61**	81.94, **+0.44**
Non-agriculture	279.37, **-0.12**	25.80, **-0.13**	-14.24, **-0.27**	1.63, **-0.0085**	21.24, **-0.40**	75.85, **+1.39**
Asia	287.02, **-0.13**	30.39, **-0.16**	-4.23, **-0.33**	3.19, **-0.053**	33.95, **-0.74**	55.32, **+1.44**
Europe	281.67, **-0.30**	24.82, **-0.27**	-9.29, **-0.76**	1.81, **-0.002**	24.33, **-0.13**	52.94, **-0.67**
North America	283.69, **-0.04**	27.31, **-0.01**	-11.24, **+0.06**	2.68, **+0.016**	34.78, **-0.16**	35.78, **+0.32**
South America	294.84, **+0.05**	31.27, **-0.01**	13.67, **-0.30**	3.56, **-0.008**	32.68, **-0.02**	72.16, **+1.44**
Africa	299.56, **-0.02**	36.46, **-0.10**	16.59, **+0.10**	1.95, **+0.026**	22.58, **-0.67**	121.30, **-1.49**
Antarctica and Oceania	272.46, **-0.08**	12.78, **-0.14**	-14.66, **-0.21**	1.60, **-0.10**	26.58, **-0.12**	72.63, **+2.64**

3.3.3 Continental Spatial Patterns and Regional Hotspots

The spatial distribution of temperature and precipitation extremes in the Base scenario reveals clear continental contrasts (Fig. 7; Table 2). Warmer continents such as Africa (AF) and South America (SA) also exhibit higher values of TXx and TNn, while colder regions like Antarctica and Oceania (AO) display consistently lower temperature extremes due to their extensive cold zones. Precipitation extremes show similar variation across continents. Drier regions—such as Europe (EU), AF, and AO—tend to have lower Rx1day values and experience longer dry spells, as reflected in elevated CDD, whereas wetter continents show stronger rainfall extremes and shorter dry periods.

https://doi.org/10.5194/egusphere-2025-4648
Preprint. Discussion started: 6 October 2025

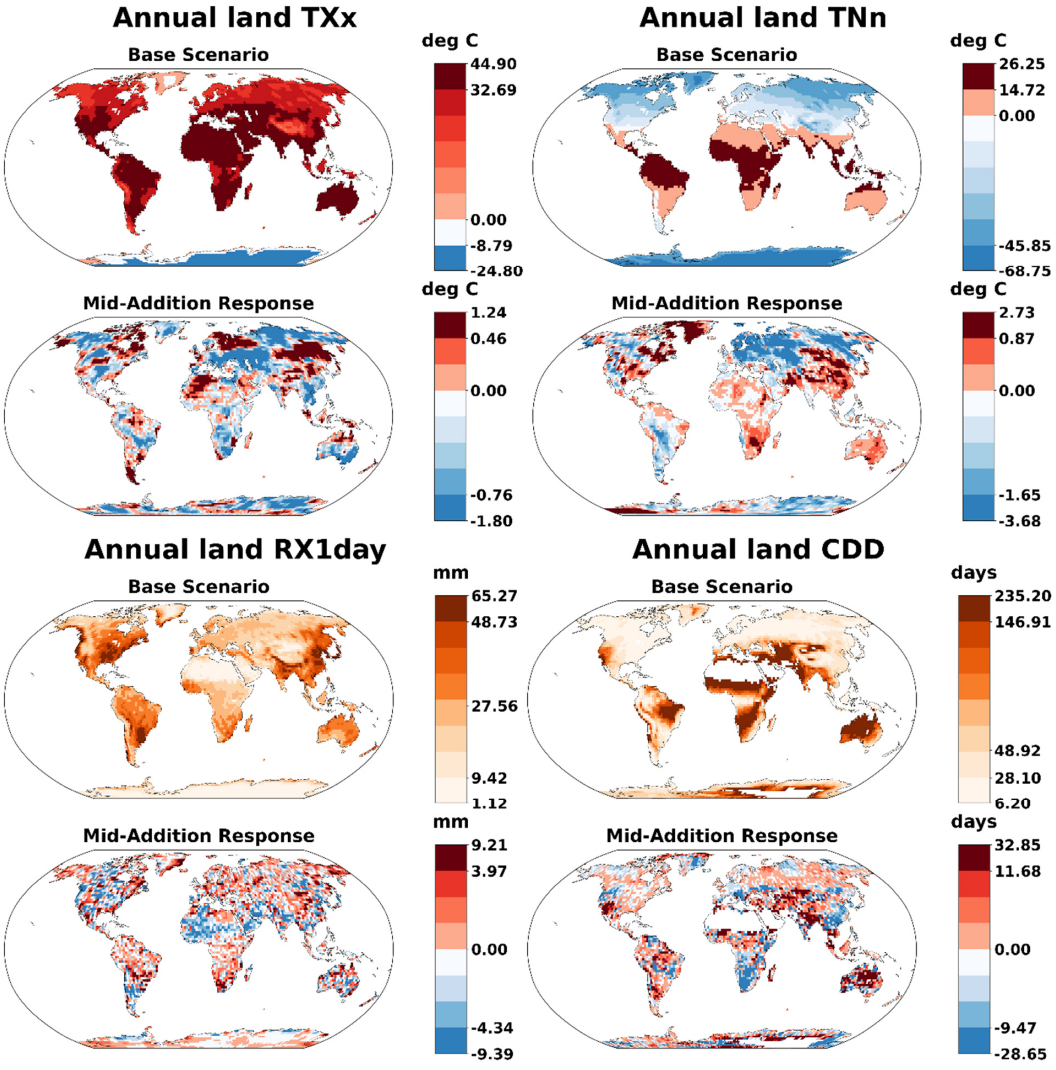

Figure 7: Climate Extremes and Their Responses to Medium Biochar Addition over Land Areas. The figure presents four climate indices: Maximum Daily Maximum Temperature (TXx), Minimum Daily Minimum Temperature (TNn), Maximum 1-Day Precipitation (Rx1day), and Consecutive Dry Days (CDD). For each index, the upper map shows the baseline values under the Base scenario for 2040–2049, calibrated using the period 2005–2014. The lower map displays the changes induced by the medium biochar addition scenario (30 t/ha). Color scales are standardized for comparability: the first color band represents values between the 95th percentile and the maximum; the last band covers the range from the 5th percentile to the minimum. All intermediate bands are evenly divided between the 5th and 95th percentiles, except for the boundary nearest to zero, which is explicitly set to zero to clearly distinguish between positive and negative values.

https://doi.org/10.5194/egusphere-2025-4648
Preprint. Discussion started: 6 October 2025

Under the medium biochar addition scenario, reductions in TXx and TNn occurred across all continents, with magnitude and spatial distribution varying by region (Figs. 7, 8, S5; Table 2). Europe experienced the strongest overall cooling (TXx −0.27 °C, TNn −0.76 °C), while Asia contributed the largest share of the global response due to its extensive land area.

Precipitation extremes displayed more heterogeneous patterns (Figs. 7, 8, S6; Table 2). Rx1day generally decreased in all continents, with the largest continental-scale reductions in Africa (−0.67 mm) and Asia (−0.74 mm). Notable hotspots included the Sahara (SAH; −1.95 mm), the Arabian Peninsula (ARP; −2.44 mm), and West Africa (WAF; −3.57 mm), where reductions exceeded approximately –2 mm.

In contrast, CDD increases are more spatially concentrated, highlighting regional hotspots of intensified drought risk. Central Australia (CAU) and the Arabian Peninsula (ARP) show exceptionally strong increases in CDD, exceeding +15 and +30 days, respectively. These two regions together account for a substantial share of the global CDD increase—approximately 50% from AO and 30% from AS (Figs. 7, 8).

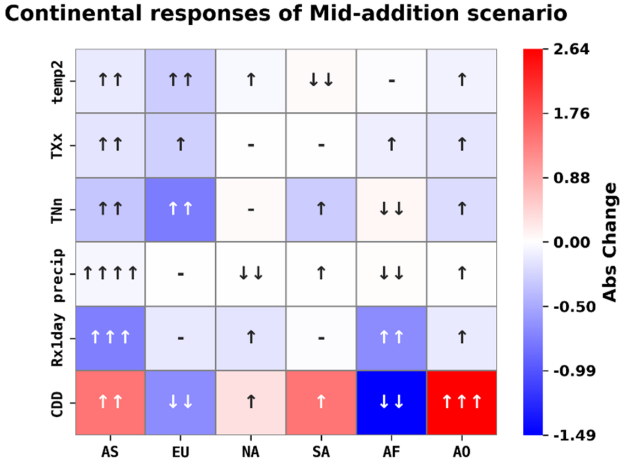

Figure 8: Continental Responses to Medium Biochar Addition (2040–2049) in Temperature and Precipitation Metrics. Each panel shows the absolute changes in: 2 m temperature (**temp2**), maximum daily maximum temperature (**TXx**), minimum daily minimum temperature (**TNn**), precipitation (**precip**), maximum 1-day precipitation (**Rx1day**), and consecutive dry days (**CDD**). Colors indicate absolute changes, and arrows indicate each continent's contribution to the total land-area response: ↑ (positive contribution) or ↓ (negative contribution) with 1 to 4 arrows representing: ↑↑↑↑/↓↓↓↓ > 100%, ↑↑↑/↓↓↓ = 50–100%, ↑↑/↓↓ = 25–50%, ↑/↓ = 5–25%; – indicates minor contribution (±5%). Total land responses are: temp2 = –0.11 K, TXx = –0.18 K, TNn = –0.25 K, precip = –0.0070 mm/day, Rx1day = –0.48 mm, and CDD = +0.99 days.

Asia exhibited strong and multifaceted responses across all temperature and precipitation extremes, making it the dominant contributor to the total land-area climate signal under medium biochar addition (Fig. 8; Table 2). This prominence reflects both its extensive land area (13.1% of global land area) and the presence of multiple high-sensitivity regions. Most of the continent

https://doi.org/10.5194/egusphere-2025-4648
Preprint. Discussion started: 6 October 2025

experienced modest cooling, with the largest reductions in TXx and TNn occurring in northern areas such as the Russian Arctic (RAR) and West Siberia (WSB), while a narrow belt between 30°N and 50°N—from the ARP to Eastern Asia (EAS)—showed slight warming (Fig. 5). Precipitation extremes declined broadly, with notable Rx1day reductions in Southeast Asia (SEA) and the Arabian Peninsula (ARP). In contrast, CDD increases were concentrated in arid and semi-arid regions, particularly ARP, which also showed the strongest Rx1day decrease, and in parts of West Central Asia (WCA) and South Asia (SAS).

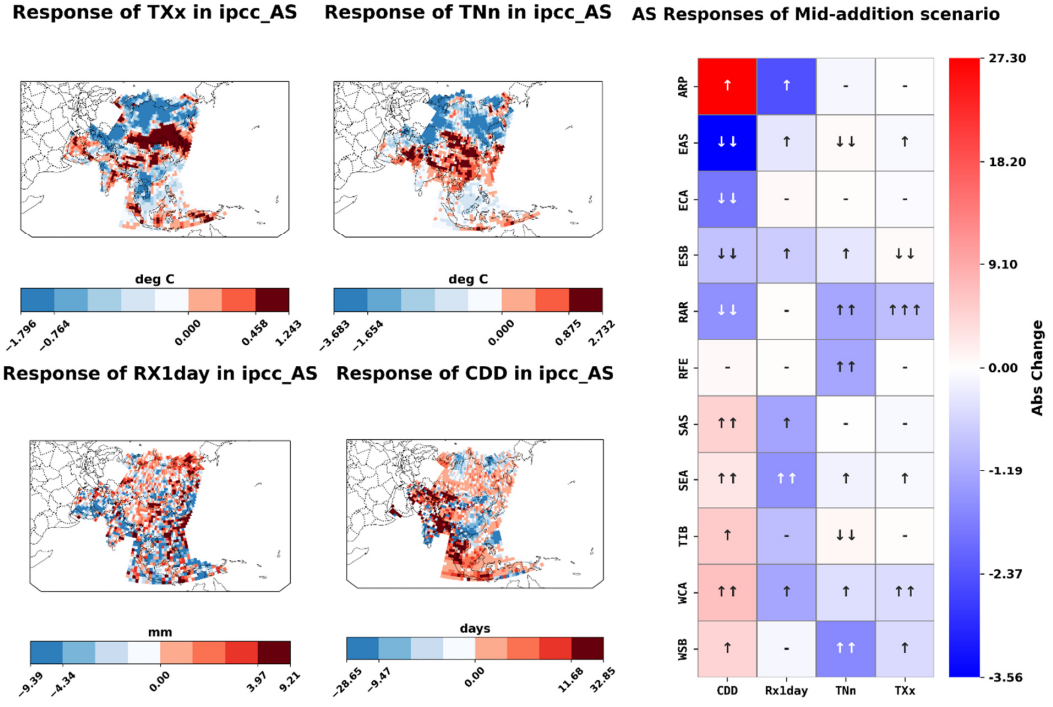

Figure 9: Regional Climate Extremes Responses to Medium Biochar Addition in Asia (30 t/ha). Maps on the left show spatial changes in maximum daily maximum temperature (TXx), minimum daily minimum temperature (TNn), maximum 1-day precipitation (Rx1day), and consecutive dry days (CDD) over Asia. Color scales are standardized across all maps: the top band represents values between the 95th percentile and the maximum, and the bottom band covers the 5th percentile to the minimum. Intermediate bands are evenly spaced between the 5th and 95th percentiles, with the boundary nearest zero fixed at zero to clearly separate positive and negative values. The heatmap on the right summarizes the regional mean responses (based on IPCC AR6 reference regions; see Fig. S1). Cell colors show absolute changes; arrows indicate each region's contribution to the response of Asia: ↑ (positive contribution) or ↓ (negative contribution) with 1 to 4 arrows representing: ↑↑↑↑/↓↓↓↓ > 100%, ↑↑↑/↓↓↓ = 50–100%, ↑↑/↓↓ = 25–50%, ↑/↓ = 5–25%; – indicates minor contribution (±5%). Asian-wide responses: TXx = –0.16 °C, TNn = –0.33 °C, Rx1day = –0.74 mm, CDD = +1.44 days.

https://doi.org/10.5194/egusphere-2025-4648
Preprint. Discussion started: 6 October 2025

4 Discussion

4.1 Biochar induced changes in soil properties

By implementation of biochar's influence on soil physical properties via increases in soil organic carbon (SOC), the pedo-transfer function (PTF) approach employed in this study captures the first-order effects of biochar addition on key soil physical properties, including porosity, field capacity, saturated hydraulic conductivity, and thermal conductivity. The direction of changes—particularly the increase in soil water retention and reduction in thermal conductivity—is consistent with results from laboratory and field experiments (Table 1). However, while the model successfully replicates the qualitative trends, it underestimates the magnitude of changes commonly reported in empirical studies. This suggests that the PTF-based approach may oversimplify the complex mechanisms through which biochar alters soil properties by attributing all changes solely to increases in SOC.

Two key factors are widely recognized as regulators of biochar's influence on soil physical properties. First, a positive relationship between biochar application rate and the magnitude of soil property changes has been reported across a range of studies (Blanco-Canqui 2017; Edeh, et al. 2020), and this dose–response relationship is partially reproduced in our simulations (Table 1). This pattern supports the role of SOC accumulation and replacement of mineral matrix in driving hydrophysical shifts. Second, biochar's effects are often modulated by soil texture, with sandy soils typically showing stronger responses than clay- or silt-dominated soils (Blanco-Canqui 2017; Edeh, et al. 2020; Omondi, et al. 2016; Razzaghi, et al. 2020). However, our model results do not consistently reproduce this texture dependence (data not shown), implying that factors beyond SOC content—such as biochar morphology, particle size distribution, and local soil microstructure—may be critical drivers. Since current PTFs do not capture these context-specific interactions, future efforts should focus on refining PTFs or developing new parameterizations that incorporate biochar-specific mechanisms beyond SOC-mediated effects (Van Looy, et al. 2017).

4.2 Biochar Effects on Global water cycle and energy balance

The soil physical property changes quantified in Section 4.1 influence how the land surface interacts with the atmosphere, yet few studies have examined these biophysical impacts within a global Earth system modeling framework.

In our simulations, biochar-induced changes in soil properties led to consistent increases in soil wetness across scenarios, confirming the first part of our first hypothesis. However, this did not translate into a corresponding increase in evapotranspiration or latent heat flux, thereby rejecting the second part of the hypothesis. Contrary to expectations, we observed only minor and spatially inconsistent changes in evaporation and related fluxes at the global scale. These results suggest that the enhanced soil water retention from biochar is not sufficient to significantly intensify the hydrological cycle on a large scale.

Instead, the most coherent responses were observed in sensible heat flux, near-surface humidity, and cloud cover—particularly over land. These patterns indicate that the dominant pathway for biochar–climate interactions operate not through enhanced evaporative cooling, but through redistribution of sensible heat and modulation of atmospheric boundary layer dynamics.

https://doi.org/10.5194/egusphere-2025-4648
Preprint. Discussion started: 6 October 2025

Increases in surface humidity and reductions in outgoing longwave radiation suggest that the observed surface cooling may be driven by atmospheric feedbacks, rather than by soil moisture fluxes alone.

Similar global and regional studies investigating the effects of soil property changes on climate also report limited global-scale impacts but notable regional variability. Soil moisture influences land-atmosphere interactions, affecting evapotranspiration, surface temperature and precipitation (Seneviratne, et al. 2010). However, the relationships between precipitation, evapotranspiration, and soil moisture are highly complex and localized, with strong regional and seasonal variations (Li, et al. 2024; Yang, et al. 2018; Zhou, et al. 2021). While these interactions are generally well-represented in climate models, their spatial and temporal complexities make it challenging to establish consistent large-scale patterns [35]. In particular, soil moisture feedbacks tend to be strongest in drylands, where hydrological limitations amplify land-atmosphere coupling effects (Zhou, et al. 2021; Swann, et al. 2012). This aligns with our findings, in which biochar-induced soil changes produced limited global-scale effects but stronger regional responses.

Although biochar effects on individual water and energy fluxes appear small and unstructured at the global level, the net energy and water balance terms—represented by top-of-atmosphere radiation (TOA) and net freshwater flux—show more consistent and systematic responses. These patterns are particularly evident over land, suggesting that integrated effects may converge even when individual components do not. The mechanisms underlying this convergence warrant further investigation, but our results indicate that biochar-induced land surface changes induced can exert coherent effects on the Earth system's energy and water budgets, albeit in subtle and regionally variable ways.

4.3 Biochar Effects on Future Climate Change

Although the mechanisms differed from initial expectations, biochar addition generally produced modest cooling and dampened extreme heat and heavy precipitation events, particularly over land. While changes in mean temperature and precipitation were spatially variable and lacked a consistent global pattern, extreme indices showed more uniform land-based responses across all scenarios: TXx, TNn, and Rx1day decreased, whereas CDD responses were more variable and driven by key hotspot regions. This suggests that biochar effects are more evident in extreme events than in mean climate variables, particularly where land-atmosphere coupling is strongest (Seneviratne, et al. 2010), consistent with earlier studies showing local-scale effects of soil property changes on heat extremes (Ganeshi, et al. 2023; Whan, et al. 2015) but limited large-scale impacts (Feng, et al. 2023).

The most consistent response was the reduction in temperature extremes, especially nighttime minima (TNn), indicating potential for mitigating heat stress. These reductions appear linked to changes in sensible heat flux, humidity, and cloud cover rather than enhanced latent heat flux. Increased soil moisture likely raised near-surface humidity and cloudiness, limiting daytime heating and reducing nighttime radiative cooling. This mechanism explains the concurrent declines in TXx and TNn and aligns with earlier findings on soil moisture buffering of temperature extremes (Schwingshackl, et al. 2017). In contrast, precipitation extremes were more variable. Rx1day declined across most land regions without altering mean annual precipitation, suggesting a shift toward a more even rainfall distribution rather than changes in total water availability.

https://doi.org/10.5194/egusphere-2025-4648
Preprint. Discussion started: 6 October 2025

The climate impacts of biochar addition also showed strong regional variability. Cold regions, including the Russian Arctic, West Siberia, and Eastern and Western Europe, exhibited the largest temperature extreme reductions, likely due to low baseline solar radiation, high temperature–radiation sensitivity and strong land–atmosphere coupling. Precipitation extremes responded most strongly in arid and coastal regions. CDD increases in areas such as the Arabian Peninsula and Central Australia suggest that biochar-induced soil changes may be insufficient to offset drought risk in moisture-limited environments, where low initial soil moisture amplifies the effects of changes in the water and energy balance. Meanwhile, coastal and monsoon-influenced regions, including West Africa, Southeast Asia, and South Asia, showed notable shifts in extreme rainfall patterns, likely driven by changes in atmospheric moisture transport and convective activity. These diverse responses reflects the complex interactions between soil moisture dynamics, atmospheric circulation, and regional hydroclimatic variability, making it difficult to isolate biochar's role in drought regulation (Yang, et al. 2018), underscoring the need for region-specific application strategies that account for local hydroclimatic conditions when evaluating biochar's role in climate adaptation.

4.3 Limitation and outlook

While our study provides valuable insights into biochar-induced changes in soil properties and their potential climate impacts, several limitations must be acknowledged.

First, our approach treated biochar as equivalent to conventional SOC in PTFs, ignoring its distinct physical and chemical characteristics such as porosity, particle size, surface reactivity, and hydrophobicity. These properties can influence soil–water–air interactions in ways that differ substantially from those of natural organic matter. By neglecting these effects, our simulations likely underestimate the full range of biochar's influence on soil hydrology and thermal dynamics.

Second, we only simulated the effects of biochar addition on soil physical properties, without representing its direct role in the carbon (C) cycle. Biochar can substantially enhance crop yields and primary productivity in the short term, while its long-term carbon sequestration potential may affect land–atmosphere CO_2 fluxes and alter global carbon budgets (Schmidt, et al. 2021; Lehmann, et al. 2021). In our experiments, the absence of biochar-driven C cycle changes meant that no significant effects on future CO_2 concentrations or CO_2-related climate feedbacks were captured. Future studies should incorporate full carbon cycle interactions to better assess biochar's combined biogeophysical and biogeochemical climate impacts.

Third, the complex interactions between the water and energy cycles present challenges in quantifying biochar's climate effects in Earth system models (Schwingshackl, et al. 2017; Santanello, et al. 2018). While biochar addition increased soil wetness, consistent global patterns in evaporation, heat fluxes, and temperature were not observed. Several factors may contribute to this uncertainty: the small fraction of agricultural land (11%), relatively minor soil property modifications (<2.5%), and intricate model feedbacks involving soil moisture, heat fluxes, and atmospheric circulation that may redistribute or dampen local effects, making direct cause–effect attribution difficult.

Additionally, our study did not conduct a comprehensive analysis of intervariable correlations, interannual variability, or climate feedback mechanisms due to time constraints. Future research should apply detailed sensitivity analyses, interannual variability assessments, and long-term trend evaluations to better understand how biochar-induced soil changes influence

https://doi.org/10.5194/egusphere-2025-4648
Preprint. Discussion started: 6 October 2025

climate variability and extreme events. Higher-resolution regional modeling could further clarify localized biochar effects, particularly in regions where land-atmosphere coupling is strongest.

5 Conclusions

This study assessed the potential influence of biochar-induced modifications in soil properties on future climate, with a particular focus on extreme climate events. Using simulations from the Max Planck Institute Earth System Model (MPI-ESM), we examined how biochar-driven changes in soil hydrological and thermal characteristics could affect temperature, precipitation, and associated extremes between 2040 and 2049.

Our first hypothesis—that biochar addition would increase soil porosity and water retention, leading to enhanced evapotranspiration, greater latent heat flux, and reduced sensible heat flux—was only partially supported. While biochar consistently increased soil wetness in a dose-dependent manner, it did not produce systematic increases in evapotranspiration or latent heat flux. Instead, the dominant response pathway involved changes in sensible heat flux, near-surface humidity, and cloud cover, indicating that atmospheric feedbacks played a more important role than evaporative cooling in driving surface temperature changes.

Our second hypothesis—that higher biochar application rates would amplify these effects—was not consistently supported at the global scale. We found no clear dose-dependent changes in global mean temperature or precipitation. However, land areas, where land–atmosphere coupling is stronger, exhibited more structured and sometimes stronger responses, particularly in climate extremes. Biochar addition consistently reduced the annual maximum daily maximum temperature (TXx) and annual minimum daily minimum temperature (TNn) over land, with a stronger cooling effect at night (TNn). These reductions were most pronounced in high-latitude and cold regions such as Eastern and Western Europe, the Russian Arctic, and West Siberia, where strong coupling between soil moisture and surface energy flux amplified the response.

Our third hypothesis—that biochar would mitigate both temperature and precipitation extremes with more pronounced effects over land—was partially supported. Temperature extremes showed consistent reductions over land across all scenarios, but precipitation extremes were more variable. While the annual maximum 1-day precipitation (Rx1day) consistently decreased over land, consecutive dry days (CDD) displayed no coherent global pattern and even increased in some arid regions, suggesting potential drought risks in moisture-limited environments. This highlights that biochar's influence on precipitation extremes is more complex and region-specific than its impact on temperature extremes.

Overall, our findings suggest that biochar's biophysical effects on mitigating future climate extremes can be substantial at the regional scale—particularly over land and in climate-sensitive regions—even though its influence on global mean temperature and precipitation remains subtle. These results highlight the importance of region-specific biochar application strategies that account for local hydroclimatic conditions. Integrating both biophysical and biogeochemical pathways into future Earth system model studies, together with high-resolution regional simulations and variability analyses, will be essential to fully assess biochar's role in climate mitigation and adaptation. As societies face mounting challenges from climate change, understanding

https://doi.org/10.5194/egusphere-2025-4648
Preprint. Discussion started: 6 October 2025

and optimizing such nature-based solutions could play a critical role in enhancing resilience and safeguarding vulnerable communities.

Code and data availability. The primary data are available via the German Climate Computing Center long-term archive for documentation **(URL: [to be inserted])**. The MPI-ESM model is managed by the Max Planck Institute for Meteorology and can be openly accessed via the DOI (https://doi.org/10.17617/3.H44EN5). The scripts used in the analysis and other supplementary information that may be useful in reproducing the authors' work are available upon request from the corresponding author.

Author contribution. CB conceived the study. LY and CB designed the experiment. TK and LY prepared the model inputs. LY performed simulations and conducted analysis. LY, CB, CK and MJK participated in the discussion of the analysis. All authors contributed to and reviewed the manuscript.

Competing interests. The contact author has declared that none of the authors have any competing interests.

Acknowledgement. We gratefully acknowledge the support of Veronika Gayler from the Max Planck Institute for Meteorology for her technical support and help during the model configuration and preparation process.

Financial support. LY was funded by the Deutsche Forschungsgemeinschaft (DFG, German Research Foundation) under Germany's Excellence Strategy - EXC 2037 'CLICCS - Climate, Climatic Change, and Society' - Project Number: 390683824.

References

IPCC: *Climate Change 2021: The Physical Science Basis. Contribution of Working Group I to the Sixth Assessment Report of the Intergovernmental Panel on Climate Change,* Edited by Vol. In Press, Cambridge University Press, 2021.

FAO: The Impact of Disasters on Agriculture and Food Security 2023 – Avoiding and reducing losses through investment in resilience. 168 (Rome, Italy, 2023).

Furtak, K. & Wolińska, A.: The impact of extreme weather events as a consequence of climate change on the soil moisture and on the quality of the soil environment and agriculture – A review, *CATENA*, **231**, 107378,https://doi.org/https://doi.org/10.1016/j.catena.2023.107378, 2023.

Praveen, B. & Sharma, P.: A review of literature on climate change and its impacts on agriculture productivity, *Journal of Public Affairs*, **19**, e1960,https://doi.org/https://doi.org/10.1002/pa.1960, 2019.

Chenu, C. *et al.*: Increasing organic stocks in agricultural soils: Knowledge gaps and potential innovations, *Soil and Tillage Research*, **188**, 41–52,https://doi.org/https://doi.org/10.1016/j.still.2018.04.011, 2019.

IPCC: in *Climate Change 2022 – Impacts, Adaptation and Vulnerability: Working Group II Contribution to the Sixth Assessment Report of the Intergovernmental Panel on Climate Change* (ed Change Intergovernmental Panel on Climate) 713–906 (Cambridge University Press, 2023).

https://doi.org/10.5194/egusphere-2025-4648
Preprint. Discussion started: 6 October 2025

Blanco-Canqui, H.: Biochar and Soil Physical Properties, *Soil Science Society of America Journal*, **81**, 687–711,https://doi.org/https://doi.org/10.2136/sssaj2017.01.0017, 2017.

Edeh, I. G., Mašek, O. & Buss, W.: A meta-analysis on biochar's effects on soil water properties – New insights and future research challenges, *Science of The Total Environment*, **714**, 136857,https://doi.org/https://doi.org/10.1016/j.scitotenv.2020.136857, 2020.

Omondi, M. O. *et al.*: Quantification of biochar effects on soil hydrological properties using meta-analysis of literature data, *Geoderma*, **274**, 28–34,https://doi.org/https://doi.org/10.1016/j.geoderma.2016.03.029, 2016.

Razzaghi, F., Obour, P. B. & Arthur, E.: Does biochar improve soil water retention? A systematic review and meta-analysis, *Geoderma*, **361**, 114055,https://doi.org/https://doi.org/10.1016/j.geoderma.2019.114055, 2020.

Usowicz, B., Lipiec, J., Łukowski, M., Marczewski, W. & Usowicz, J.: The effect of biochar application on thermal properties and albedo of loess soil under grassland and fallow, *Soil and Tillage Research*, **164**, 45–51,https://doi.org/https://doi.org/10.1016/j.still.2016.03.009, 2016.

Zhang, Q. *et al.*: Effects of Biochar Amendment on Soil Thermal Conductivity, Reflectance, and Temperature, *Soil Science Society of America Journal*, **77**, 1478–1487,https://doi.org/https://doi.org/10.2136/sssaj2012.0180, 2013.

Zhao, J., Ren, T., Zhang, Q., Du, Z. & Wang, Y.: Effects of Biochar Amendment on Soil Thermal Properties in the North China Plain, *Soil Science Society of America Journal*, **80**, 1157–1166,https://doi.org/https://doi.org/10.2136/sssaj2016.01.0020, 2016.

Hossain, M. Z. *et al.*: Biochar and its importance on nutrient dynamics in soil and plant, *Biochar*, **2**, 379–420,https://doi.org/10.1007/s42773-020-00065-z, 2020.

Schmidt, H.-P. *et al.*: Biochar in agriculture – A systematic review of 26 global meta-analyses, *GCB Bioenergy*, **13**, 1708–1730,https://doi.org/https://doi.org/10.1111/gcbb.12889, 2021.

Shrestha, R. K. *et al.*: Biochar as a negative emission technology: A synthesis of field research on greenhouse gas emissions, *Journal of Environmental Quality*, **52**, 769–798,https://doi.org/https://doi.org/10.1002/jeq2.20475, 2023.

Van Looy, K. *et al.*: Pedotransfer Functions in Earth System Science: Challenges and Perspectives, *Reviews of Geophysics*, **55**, 1199–1256,https://doi.org/https://doi.org/10.1002/2017RG000581, 2017.

Koster, R. D. *et al.*: Regions of Strong Coupling Between Soil Moisture and Precipitation, *Science*, **305**, 1138–1140,https://doi.org/10.1126/science.1100217, 2004.

Lorenz, K. & Lal, R.: Biochar application to soil for climate change mitigation by soil organic carbon sequestration, *Journal of Plant Nutrition and Soil Science*, **177**, 651–670,https://doi.org/https://doi.org/10.1002/jpln.201400058, 2014.

Seneviratne, S. I. *et al.*: Investigating soil moisture–climate interactions in a changing climate: A review, *Earth-Science Reviews*, **99**, 125–161,https://doi.org/https://doi.org/10.1016/j.earscirev.2010.02.004, 2010.

Woolf, D., Amonette, J. E., Street-Perrott, F. A., Lehmann, J. & Joseph, S.: Sustainable biochar to mitigate global climate change, *Nature Communications*, **1**, 56,https://doi.org/10.1038/ncomms1053, 2010.

Grant, L. *et al.*: Global emergence of unprecedented lifetime exposure to climate extremes, *Nature*, **641**, 374–379,https://doi.org/10.1038/s41586-025-08907-1, 2025.

Kwon, M. J., Ciais, P., Bastos, A. & Beer, C.: Legacy Effects of the Siberian Heatwave of 2020 on Above- and Belowground Processes, *Global Biogeochemical Cycles*, **39**, e2025GB008607,https://doi.org/https://doi.org/10.1029/2025GB008607, 2025.

Tian, Y. *et al.*: Characterizing heatwaves based on land surface energy budget, *Communications Earth & Environment*, **5**, 617,https://doi.org/10.1038/s43247-024-01784-y, 2024.

Varney, R. M., Chadburn, S. E., Burke, E. J. & Cox, P. M.: Evaluation of soil carbon simulation in CMIP6 Earth system models, *Biogeosciences*, **19**, 4671–4704,https://doi.org/10.5194/bg-19-4671-2022, 2022.

Lehmann, J. *et al.*: Biochar in climate change mitigation, *Nature Geoscience*, **14**, 883–892,https://doi.org/10.1038/s41561-021-00852-8, 2021.

Eyring, V. *et al.*: Overview of the Coupled Model Intercomparison Project Phase 6 (CMIP6) experimental design and organization, *Geosci. Model Dev.*, **9**, 1937–1958,https://doi.org/10.5194/gmd-9-1937-2016, 2016.

Mauritsen, T. *et al.*: Developments in the MPI-M Earth System Model version 1.2 (MPI-ESM1.2) and Its Response to Increasing CO2, *Journal of Advances in Modeling Earth Systems*, **11**, 998–1038,https://doi.org/https://doi.org/10.1029/2018MS001400, 2019.

https://doi.org/10.5194/egusphere-2025-4648
Preprint. Discussion started: 6 October 2025

Reick, C. H. *et al.*: JSBACH 3 The land component of the MPI Earth System Model Documentation of version 3.2. (Max Planck Institute for Meteorology, Hamburg, 2021).

Poggio, L. *et al.*: SoilGrids 2.0: producing soil information for the globe with quantified spatial uncertainty, *SOIL*, **7**, 217–240,https://doi.org/10.5194/soil-7-217-2021, 2021.

Lawrence, D. M. & Slater, A. G.: Incorporating organic soil into a global climate model, *Climate Dynamics*, **30**, 145–160,https://doi.org/10.1007/s00382-007-0278-1, 2008.

Saxton, K. E. & Rawls, W. J.: Soil Water Characteristic Estimates by Texture and Organic Matter for Hydrologic Solutions, *Soil Science Society of America Journal*, **70**, 1569–1578,https://doi.org/10.2136/sssaj2005.0117, 2006.

Harper, K. L. *et al.*: A 29-year time series of annual 300m resolution plant-functional-type maps for climate models, *Earth Syst. Sci. Data*, **15**, 1465–1499,https://doi.org/10.5194/essd-15-1465-2023, 2023.

Karl, T. R., Nicholls, N. & Ghazi, A.: in *Weather and Climate Extremes: Changes, Variations and a Perspective from the Insurance Industry* (eds Thomas R. Karl, Neville Nicholls, & Anver Ghazi) 3–7 (Springer Netherlands, 1999).

Li, N., Skaggs, T. H., Ellegaard, P., Bernal, A. & Scudiero, E.: Relationships among soil moisture at various depths under diverse climate, land cover and soil texture, *Science of The Total Environment*, **947**, 174583,https://doi.org/https://doi.org/10.1016/j.scitotenv.2024.174583, 2024.

Yang, L., Sun, G., Zhi, L. & Zhao, J.: Negative soil moisture-precipitation feedback in dry and wet regions, *Scientific Reports*, **8**, 4026,https://doi.org/10.1038/s41598-018-22394-7, 2018.

Zhou, S. *et al.*: Soil moisture–atmosphere feedbacks mitigate declining water availability in drylands, *Nature Climate Change*, **11**, 38–44,https://doi.org/10.1038/s41558-020-00945-z, 2021.

Swann, A. L. S., Fung, I. Y. & Chiang, J. C. H.: Mid-latitude afforestation shifts general circulation and tropical precipitation, *Proceedings of the National Academy of Sciences*, **109**, 712–716,https://doi.org/10.1073/pnas.1116706108, 2012.

Ganeshi, N. G. *et al.*: Soil moisture revamps the temperature extremes in a warming climate over India, *npj Climate and Atmospheric Science*, **6**, 12,https://doi.org/10.1038/s41612-023-00334-1, 2023.

Whan, K. *et al.*: Impact of soil moisture on extreme maximum temperatures in Europe, *Weather and Climate Extremes*, **9**, 57–67,https://doi.org/https://doi.org/10.1016/j.wace.2015.05.001, 2015.

Feng, Y., Wang, H., Liu, W. & Sun, F.: Global Soil Moisture–Climate Interactions during the Peak Growing Season, *Journal of Climate*, **36**, 1187–1196,https://doi.org/https://doi.org/10.1175/JCLI-D-22-0161.1, 2023.

Schwingshackl, C., Hirschi, M. & Seneviratne, S. I.: Quantifying Spatiotemporal Variations of Soil Moisture Control on Surface Energy Balance and Near-Surface Air Temperature, *Journal of Climate*, **30**, 7105–7124,https://doi.org/https://doi.org/10.1175/JCLI-D-16-0727.1, 2017.

Santanello, J. A. *et al.*: Land–Atmosphere Interactions: The LoCo Perspective, *Bulletin of the American Meteorological Society*, **99**, 1253–1272,https://doi.org/https://doi.org/10.1175/BAMS-D-17-0001.1, 2018.